Catalysis Science & Technology

PAPER

View Article Online
View Journal | View Issue

Cite this: *Catal. Sci. Technol.*, 2015, 5, 1323

Factors influencing the catalytic oxidation of benzyl alcohol using supported phosphine-capped gold nanoparticles†

Rohul H. Adnan,[ab] Gunther G. Andersson,[c] Matthew I. J. Polson,[a] Gregory F. Metha[d] and Vladimir B. Golovko*[ae]

Received 10th September 2014,
Accepted 19th November 2014

DOI: 10.1039/c4cy01168f

www.rsc.org/catalysis

Two phosphine-stabilised gold clusters, $Au_{101}(PPh_3)_{21}Cl_5$ and $Au_9(PPh_3)_8(NO_3)_3$, were deposited and activated on anatase TiO_2 and fumed SiO_2. These catalysts showed an almost complete oxidation of benzyl alcohol (>90%) within 3 hours at 80 °C and 3 bar O_2 in methanol with a high substrate-to-metal molar ratio of 5800 and turn-over frequency of 0.65 s^{-1}. Factors influencing catalytic activity were investigated, including metal–support interaction, effects of heat treatments, chemical composition of gold clusters, the size of gold nanoparticles and catalytic conditions. It was found that the anions present in gold clusters play a role in determining the catalytic activity in this reaction, with NO_3^- diminishing the catalytic activity. High catalytic activity was attributed to the formation of large gold nanoparticles (>2 nm) that coincides with partial removal of ligands which occurs during heat treatment and catalysis. Selectivity towards the formation of methyl benzoate can be tuned by selection of the reaction temperature. The catalysts were characterised using transmission electron microscopy, UV-vis diffuse reflectance spectroscopy and X-ray photoelectron spectroscopy.

1 Introduction

For centuries, gold was considered to be chemically inert and catalytically inactive, making it valuable in jewellery and as coinage metal but worthless for applications in catalysis. However, this perception has changed since the early report by Haruta *et al.* that small gold particles were catalytically active in CO oxidation at low temperature[1] and the discovery by Hutchings *et al.* that a gold-based catalyst could be used in the hydrochlorination of acetylene.[2] These discoveries triggered a revolution in gold-based catalysis, with numerous follow-up papers demonstrating the superiority of gold-based catalysts over the more expensive platinum group metals in various catalytic processes, with improvements in activity, selectivity and stability against deactivation paving a pathway to numerous commercially-oriented patents.[3,4] The number of studies on nanoparticulate gold-based catalysts for a broad range of bulk and fine chemical synthesis processes has grown exponentially.[1,5–8]

Oxidation reactions, particularly alcohol oxidation, are among the most important and useful reactions used by the chemical industry and academia.[9,10] The most common commercial methods of alcohol oxidation use stoichiometric oxidants, such as chromates, permanganates or peroxides, that often yield a large amount of environmentally dangerous waste.[11] The use of harmful organic solvents (*e.g.* chlorinated solvents) may also have a negative environmental impact.[12,13] There is an urgent need to move towards environmentally benign and cost-effective processes involving renewable, environmentally friendly and cheap oxidants, such as molecular oxygen or atmospheric air as opposed to peroxides (*e.g.* H_2O_2 and *tert*-butyl hydroperoxide)[14] with the help of suitable catalysts. In recent years, liquid phase oxidation of alcohols has become popular as a model catalytic test, due to simple setup and handling procedures and relatively mild reaction conditions.[15,16] Supported platinum group catalysts are widely used in the oxidation of alcohols, yet they often require a secondary metal as a promoter to increase the selectivity and stability of such catalysts.[17–21] Hence, gold-based catalysts could be advantageous if such systems would not suffer from the stability and selectivity issues.[22]

A systematic study of the nature of the active sites is crucial in improving the activity and selectivity of catalysts

[a] *Department of Chemistry, University of Canterbury, Christchurch, 8041, New Zealand. E-mail: vladimir.golovko@canterbury.ac.nz*
[b] *Chemistry Department, University of Malaya, Kuala Lumpur, 50603, Malaysia*
[c] *Flinders Centre for Nanoscale Science and Technology, Flinders University, Adelaide, SA 5001, Australia*
[d] *Department of Chemistry, University of Adelaide, Adelaide, SA 5005, Australia*
[e] *The MacDiarmid Institute for Advanced Materials and Nanotechnology, PO Box 600, Wellington, 6140, New Zealand*

† Electronic supplementary information (ESI) available: The experimental details about synthesis of the gold clusters and the characterisations are available. See DOI: 10.1039/c4cy01168f

towards the formation of the desired partial oxidation products. In the case of heterogeneous Au-based catalysts, the following factors are often considered to define catalytic activity and selectivity: gold particle size and morphology, oxidation state of gold species, metal–support interaction and specific parameters of catalytic testing conditions. The nature of the active site in the liquid phase oxidation of alcohols is currently still unclear, with both ultra-small particles (<2 nm)[23,24] and larger particles (>2 nm)[25] reported as active catalysts. Tsukuda *et al.* reported that as the size of gold nanoparticles reduced below 2 nm, the turnover frequency (TOF) for the aerobic oxidation of *p*-hydroxybenzylalcohol increased significantly.[26] The authors proposed that the catalytic activity of these small gold nanoparticles was due to the increased electron density on the gold core and also charge transfer from the poly(*N*-vinyl-2-pyrrolidone) ligands. However, Haider *et al.* observed that smaller size was not necessarily responsible for higher activity – the authors reported that the optimum size of the gold nanoparticles for ethanol oxidation is *ca.* 7 nm, irrespective of the supports.[25] Zheng *et al.* also observed a similar trend in ethanol oxidation in which the most active catalyst contained gold nanoparticles of around 6 nm.[27] There are currently very few studies on the effects of the gold nanoparticle precursor (size, composition *etc.*) on the performance of resulting catalysts since the majority of reports in the literature are focused predominantly on the morphology and size of gold nanoparticles.[23,28–30] Only recently, several studies on the effects of ligands, such as citrate, polyvinylpyrrolidone and polyvinyl alcohol, on the performance of gold-based catalysts have been reported in a wide range of catalytic reactions – glycerol oxidation,[31] hydrogenation of cinnamaldehyde[32] and reduction of *p*-nitrophenol.[33] These findings clearly suggest that the nature of ligands plays a critical role in determining the performance of the catalytically active gold particles in a particular reaction, perhaps, similarly to the role of support.[34] Hence, it is important to study the effect of the composition (size of the gold core, neutral organic ligands and anionic ligands or counterions) of precursors used in fabrication of gold-based catalysts in order to design catalysts with high activity and improved selectivity.

Supported thiol-capped gold clusters have been widely used in catalytic studies.[35–37] For example, Jin *et al.* supported $Au_{25}(SR)_{18}$, $Au_{38}(SR)_{24}$ and $Au_{99}(SPh)_{42}$ clusters on various metal oxides and tested them in selective oxidation and hydrogenation reactions.[38–41] Tsukuda *et al.* used $Au_{10}(SG)_{10}$, $Au_{18}(SG)_{14}$, $Au_{25}(SG)_{18}$ and $Au_{39}(SG)_{24}$ deposited on hydroxyapatite in styrene oxidation.[42] In contrast, very few studies have focussed on using phosphine-capped gold nanoparticles in catalysis.[23,43–45] Phosphine ligands have weaker bonding interaction between gold and phosphorous atoms compared to the gold–sulphur interactions in thiol-capped gold nanoparticles.[46]

Building on our recent X-ray spectroscopy studies of supported triphenylphosphine-stabilised gold nanoparticles,[47,48] we hereby aim to study the catalytic performance of materials derived from selected phosphine-capped gold clusters, supported and activated on titania and silica using liquid phase benzyl alcohol oxidation as a model catalytic test. Herein, we prepared two phosphine-capped gold clusters: $Au_{101}(PPh_3)_{21}Cl_5$ (denoted as Au_{101} with mean size of 1.6 ± 0.3 nm) and $Au_9(PPh_3)_8(NO_3)_3$ (denoted as Au_9 with mean size of 0.8 nm). These clusters were then deposited and activated on TiO_2 (anatase) and SiO_2 (fumed) using sol-immobilisation method; a well-established method used by Rossi,[10] Jin[39] and Hutchings[49] for immobilising pre-synthesized gold nanoparticles or clusters onto supports. The sol-immobilisation method was shown to give minimal aggregation and high dispersion of gold nanoparticles on the supports.[50] The catalysts were then calcined under different atmospheres: oxygen (O_2) and oxygen and subsequently hydrogen (O_2–H_2) at 200 °C to dislodge the phosphine ligands and expose the metal core adsorbed on the support to facilitate access by the substrate.[47]

2 Experimental

2.1 Materials

All reactants were analytical reagent grade and used without further purification. Benzyl alcohol (>99%), benzaldehyde (>99%), methyl benzoate (99%), benzoic acid (99.7%), and anisole (>99.5% anhydrous) were purchased from Sigma Aldrich. HPLC grade methanol (99.9%, Fisher Scientific) was degassed (N_2) and dried over pre-calcined alumina prior to use. Tetrachloroauric acid was prepared using 99.99% pure gold following the procedure detailed by Brauer.[51] Triphenylphosphine-stabilised gold nanoparticles with an average estimated formula $Au_{101}(PPh_3)_{21}Cl_5$ (denoted as Au_{101}) have been synthesised according to procedure reported earlier by Weare *et al.*[52] while $Au_9(PPh_3)_8(NO_3)_3$ was made according to the protocol reported by Wen *et al.*[53] Anatase (99.5%, *ca.* 70 $m^2\ g^{-1}$, 10–30 nm particles) was purchased from SkySpring Nanomaterials. Instrument grade H_2 (99.98% with <20 ppm H_2O, BOC) and O_2 (99.2% with <10 ppm H_2O, Southern Gas Services Ltd.) were used for the calcination procedures.

2.2 Preparation of catalysts

The clusters were deposited onto the support using the protocol reported by Zhu *et al.*[38] For the purpose of this study we focused on materials with 0.17 wt% Au (*i.e.* ratio of the weight of the Au due to presence of clusters relative to the weight of support) on titania and 0.5 wt% Au on silica to give equivalent surface density of gold particles.[47]

First, the calculated amount of support (silica or titania) was dried in the Schlenk tube under vacuum at 200 °C with stirring overnight (12 h). Upon cooling to room temperature, 5.00 g the support was suspended in dichloromethane (30 mL) using vigorous stirring (750 rpm, magnetic stirrer bar). A solution of calculated amount of gold cluster (*e.g.* 11.2 mg of Au_{101}) in dichloromethane (10 mL) was added to the suspension of support under vigorous stirring at room temperature and the mixture was left stirring overnight (12 h). The mixture

was then dried in vacuum at room temperature and stored at 4 °C (untreated catalysts, labelled as Au_x/support-untreated).

Two heat treatments were employed in this work: a) calcination under pure O_2 atmosphere at 200 °C for 2 h and b) calcination under pure O_2 at 200 °C for 2 h followed by calcination in H_2 at 200 °C for 2 h.[47] All cluster deposition and activation experiments were performed using glassware wrapped in Al foil to avoid exposure of materials to light. All prepared catalysts were stored in vials wrapped in Al foil in a fridge (4 °C). For the purpose of following discussion catalysts are labelled in the following manner: "*x* wt% Au_y/support-treatment", where *x* corresponds to the weight % of pure Au and *y* = 9 or 101.

2.3 Catalytic testing

The catalytic oxidation of benzyl alcohol was performed in stainless steel autoclaves (total internal volume of 57 mL) equipped with Teflon liners and magnetic stirrers, with temperature control of the reaction achieved by using a hotplate stirrer controlled by a thermocouple immersed into the reaction mixture. Typically, a mixture of 0.270 g, 2.50 mmol benzyl alcohol and 0.135 g, 1.25 mmol anisole (internal standard) in methanol (25 mL) were charged into a Teflon liner. Then, 0.345 g, 2.50 mmol K_2CO_3 and 50 mg of catalyst were added, giving benzyl alcohol to Au molar ratio of 5800. A purge–vent cycle was completed 3 times with pure oxygen to ensure high purity of the atmosphere before the autoclave was pressurised with 5 bar of oxygen and heated to a specific temperature for the desired reaction time. At the end of a catalytic test, the reaction was stopped by cooling the autoclave to 3 °C in an ice-bath. The reaction mixture was centrifuged at 5000 rpm for 15 minutes to separate product mixture and the catalyst. The catalyst was washed with methanol (3 × 15 mL) and dried *in vacuo* prior to recycling. Each catalytic test was repeated at least in triplicate giving lower than 3% differences in conversion and selectivity.

Product mixtures were analysed using high performance liquid chromatography (HPLC) Dionex Ultimate 300 system equipped with UV detector and fitted with a Luna 5μ C18(2) (250 × 4.60 mm) reversed phase column. The products were eluted using a mixture of 0.05 v/v% trifluoroacetic acid in water (70%) and acetonitrile (30%). Gold content was measured *via* atomic absorption spectroscopy (AAS) using a Varian SpectraAA 220 FS with ASL hollow cathode lamp for the Au element.

2.4 Catalyst characterization

High resolution transmission electron microscopy (HRTEM) was performed using a Philips CM-200 system operating at 200 kV. Samples were deposited as a suspension in methanol onto Cu (300 mesh) grids coated with a holey carbon film and dried in vacuum immediately prior to TEM study. Statistical evaluation of at least 250 gold particles per sample was undertaken to estimate mean particle sizes and construct size distribution histograms. X-ray photoelectron spectroscopy (XPS) study was performed at the soft X-ray beamline at the Australian Synchrotron using a SPECS Phoibos 150 hemispherical electron analyser with the photon energy set to 690 eV. The irradiation spot size was *ca.* 600 × 600 μm, providing an X-ray flux of *ca.* 10^{12} photon mm^{-2} s^{-1}.[47] XPS samples were prepared by suspending catalysts in dichloromethane at a concentration of *ca.* 1 mg mL^{-1}. A 10 μL drop of each sample was deposited onto a clean 6 × 6 mm silicon (Si) wafer and dried in vacuum (in the dark) immediately before analysis. UV-vis diffuse reflectance spectroscopy (UV-vis DRS) spectra were recorded using a Cintra 404 (GBC Scientific Equipment) spectrophotometer. Thermogravimetric analysis (TGA) was performed using a TGA-DSC Q6000 Universal Analyser. ^{31}P NMR spectra were recorded by taking a small aliquot of the reaction mixture, dissolving it in $CDCl_3$ solvent and collecting data using an Agilent Technologies 400 Hz NMR system.

3 Results and discussion

3.1 Catalyst characterization

Au_{101} nanoparticles and Au_9 clusters are smaller than 2 nm, are highly monodisperse, have a high surface area to volume ratio, and do not have a localised surface plasmon resonance (LSPR) due to their non-metallic surface state.[46,52] We prepared heterogeneous gold catalysts derived from Au_{101} and Au_9 clusters deposited onto the surface of TiO_2 (anatase) and SiO_2 (fumed) nanopowders. The 0.17 wt% Au_{101}/TiO_2-untreated and 0.17 wt% Au_9/TiO_2-untreated catalysts made *via* the sol-immobilisation method show minimal cluster aggregation (Fig. 1a, 2a). Imaging ultra-small clusters on support, such as Au_9 on TiO_2, was very difficult due to poor contrast of the ultra-small gold particles over support material, as was emphasised by Hutching *et al.*[54] Hence, no statistical analysis of the particle size distribution was provided for 0.17 wt% Au_9/TiO_2-untreated. Although, in the case of Au_9 cluster poor contrast did not allow precise particle size determination, the absence of larger, easily visible in HRTEM aggregates is evident (Fig. 2a). Our earlier study using synchrotron XPS and NEXAS also confirmed the presence of a significant fraction of supported Au_9 clusters on TiO_2.[47] The gold loading of 0.17 wt% on TiO_2 was chosen to minimise the aggregation of gold nanoparticles, yet still to be able to obtain discernible signals in X-ray photoelectron spectroscopy (XPS) and UV-vis diffuse reflectance spectroscopy (UV-vis DRS) studies. In the case of clusters supported on fumed SiO_2, the Au loading was normalised based on the surface area (to be 0.5 wt%) in order to obtain equivalent (to TiO_2) surface coverage by clusters.

A careful heat-treatment was employed in order to remove the capping ligands and expose the gold core to the substrate, yet to minimise aggregation. Here, calcination of the catalysts was done at 200 °C under different environments: under pure oxygen (O_2) and oxygen followed by hydrogen (O_2–H_2).[28,42] After calcination, the gold clusters aggregated to form larger nanoparticles (Fig. 1 and 2).[47] TiO_2-based catalysts showed minimal aggregation and narrower particle size distributions

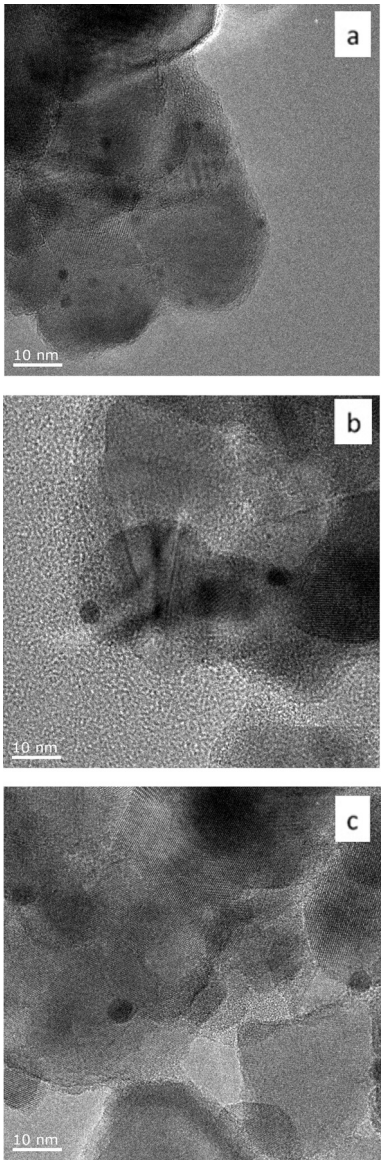

Fig. 1 Representative TEM images of 0.17 wt% Au_{101}/TiO_2 catalysts before catalytic reaction, a) Au_{101}/TiO_2-untreated, b) Au_{101}/TiO_2–O_2, and c) Au_{101}/TiO_2–O_2–H_2.

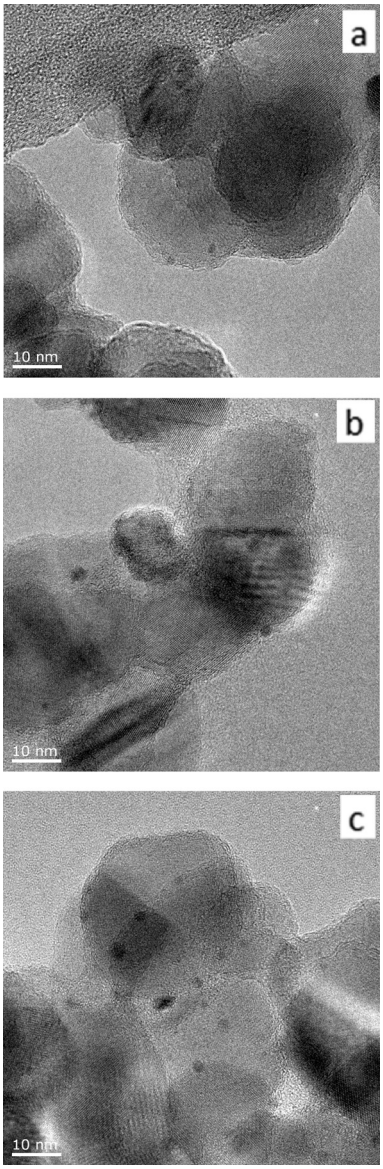

Fig. 2 Representative TEM images of 0.17 wt% Au_9/TiO_2 catalysts before catalytic reaction, a) Au_9/TiO_2-untreated, b) Au_9/TiO_2–O_2, and c) Au_9/TiO_2–O_2–H_2.

as compared to SiO_2-based catalysts, suggesting that gold formed stronger metal–support interaction with TiO_2 *cf.* SiO_2 (Fig. 1 and 3). UV-vis DR spectra (Fig. 4 and 5) showed the absence of LSPR bands in the cases of untreated catalysts allows us to infer that the gold nanoparticles were predominantly with sizes below 2 nm and retained their non-metallic state. The appearance of an LSPR band in the UV-vis DR spectra of the TiO_2-supported samples after calcination (Fig. 4 and 5) indicated formation of plasmonic gold nanoparticles which is indicative of the increase in particle size to greater than 2 nm.[55–57] It was previously reported that the position of the maximum of the LSPR band moves to longer wavelength as the size of gold particles increases, although in some cases this general trend broke down due to the effect of the dielectric constant of the surrounding environment.[58–61] Interestingly, the 0.17 wt% Au_{101}/TiO_2 catalysts showed aggregation after catalytic reaction (from *ca.* 2.0 to *ca.* 3.6 nm; Table 1). Particle size analysis based on the statistical evaluation of numerous TEM images (Table 1) confirms that the increase in particle size after heat-treatments and after catalytic reactions for Au_x/TiO_2 catalysts (x = 9, 101) was consistent with the red shift in the peak maxima position of the LSPR bands observed in UV-vis DR spectra.

For 0.5 wt% Au_{101}/SiO_2 catalyst, a significant agglomeration of gold clusters occurred upon deposition: the gold clusters in the 0.5 wt% Au_{101}/SiO_2-untreated catalyst aggregated to form gold nanoparticles of mean size 3.6 ± 1.2 nm. The observed particle size is almost twice the size of pristine Au_{101} cluster and substantially larger than the size of the gold particles (2.0 ± 0.4 nm) in the case of Au_{101} immobilized on TiO_2

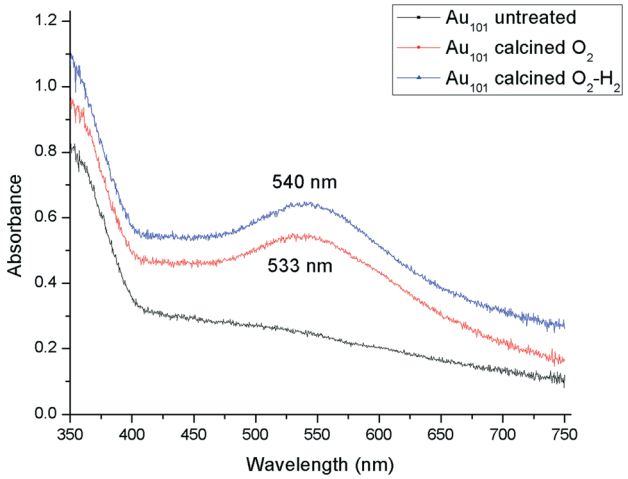

Fig. 3 UV-vis DR spectra of 0.17 wt% Au_{101}/TiO_2 catalysts.

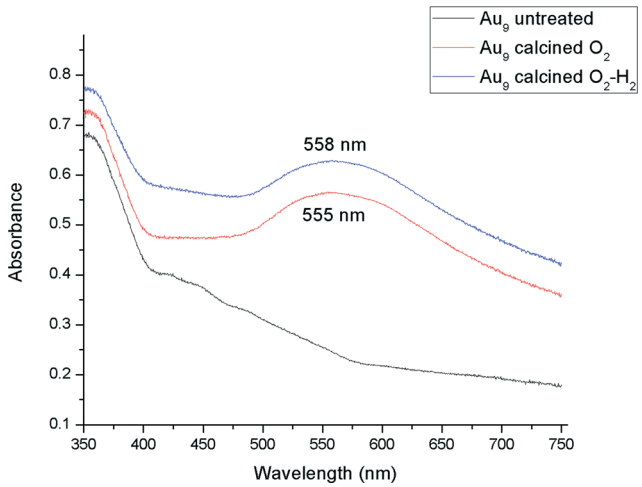

Fig. 4 UV-vis DR spectra of 0.17 wt% Au_9/TiO_2 catalysts.

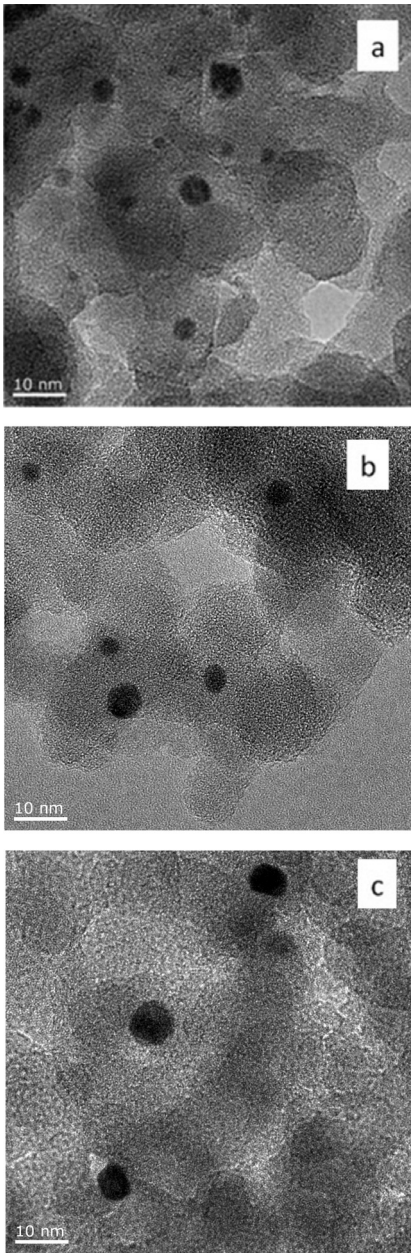

Fig. 5 Representative TEM images of 0.5 wt% Au_{101}/SiO_2 catalysts before catalytic reaction, a) Au_{101}/SiO_2-untreated, b) Au_{101}/SiO_2–O_2, and c) Au_{101}/SiO_2–O_2–H_2.

at the same surface coverage. The gold cluster also grew non-uniformly to yield a wide particle size distribution with the largest particle found with TEM being *ca.* 8 nm and the smallest being *ca.* 2 nm (Fig. 5a and S9a ESI†). After calcination under O_2 and O_2 followed by H_2 at 200 °C, the agglomeration progressed further resulting in the formation of larger gold nanoparticles with wider particle size distributions (Fig. 5(b and c) and S9(b and c) ESI†). A summary of supported gold particle mean sizes and positions of the LSPR peak maxima are given in Table 1.

Our recent XPS study of phosphine-capped Au clusters on TiO_2 showed that for untreated Au_9/TiO_2 and Au_{101}/TiO_2 a significant fraction of phosphine ligands were dislodged from the gold cores and formed phosphine oxide-like species by interaction with oxygen on the TiO_2 surface, leaving a tiny amount of phosphine ligands bound to the gold core.[47] Calcination under O_2 atmosphere detached the majority of phosphine ligands from the gold core by forming phosphine-oxide species. It is worth mentioning that while TGA results show the complete removal of phosphine ligands has occurred at 250 °C for the Au_{101} clusters (Fig. S3, ESI†) and at 240 °C for the Au_9 cluster (Fig. S6, ESI†), the phosphine ligands attached to supported Au clusters were not removed as phosphoric acid (H_3PO_4), but as phosphine-oxide species probably due to the interaction with the oxygen from TiO_2 surfaces (*e.g.* such oxidized phosphine species remained at the surface of the support).[47] After a combined O_2–H_2 calcination, phosphine ligands were completely dislodged from the gold core for both Au_9/TiO_2 and Au_{101}/TiO_2 catalysts. Our first XPS study of a wider range of ultra-small gold phosphine clusters suggests that the nature of the anionic species (Cl^- and NO_3^-) did not significantly influence

Table 1 Summary of the gold particle size and the LSPR peak maximum positions of the supported gold catalysts

Entry	Catalyst	Condition	Size[a] (nm)	LSPR peak maximum[b] (nm)
1	0.17% Au_{101}/TiO_2-untreated	Before reaction	2.0 ± 0.4	No peak
2	0.17% Au_{101}/TiO_2–O_2	Before reaction	3.5 ± 0.8	533
3	0.17% Au_{101}/TiO_2–O_2–H_2	Before reaction	4.4 ± 1.2	540
4	0.17% Au_{101}/TiO_2-untreated	After reaction	3.6 ± 1.2	540
5	0.17% Au_{101}/TiO_2–O_2	After reaction	3.9 ± 1.0	541
6	0.17% Au_{101}/TiO_2–O_2–H_2	After reaction	4.6 ± 1.5	546
7	0.17% Au_{101}/TiO_2-untreated	After recycle	4.6 ± 2.5	541
8	0.17% Au_{101}/TiO_2–O_2	After recycle	4.2 ± 1.2	547
9	0.17% Au_{101}/TiO_2–O_2–H_2	After recycle	5.0 ± 1.5	551
10	1.3% Au_{101}/TiO_2-untreated	Before reaction	2.7 ± 0.6	530
11	0.17% Au_9/TiO_2-untreated	Before reaction	<2[c]	No peak
12	0.17% Au_9/TiO_2–O_2	Before reaction	2.4 ± 0.5	555
13	0.17% Au_9/TiO_2–O_2–H_2	Before reaction	2.9 ± 0.9	558
14	0.17% Au_{101}/SiO_2-untreated	Before reaction	<2[c]	No peak
15	0.17% Au_{101}/SiO_2–O_2	Before reaction	3.6 ± 2.7	529
16	0.17% Au_{101}/SiO_2–O_2–H_2	Before reaction	4.4 ± 2.5	524
17	0.5% Au_{101}/SiO_2-untreated	Before reaction	3.6 ± 1.2	537
18	0.5% Au_{101}/SiO_2–O_2	Before reaction	4.7 ± 1.6	525
19	0.5% Au_{101}/SiO_2–O_2–H_2	Before reaction	5.7 ± 2.9	518

[a] Measured using TEM. [b] Measured using UV-vis DRS. [c] Estimated based on the absence of LSPR peak in the UV-vis DR spectra.

the position of the Au $4f_{7/2}$ peak (84.7 ± 0.1 eV for Au_{11} cluster containing Cl^- *vs.* 85.1 ± 0.1 eV for both Au_8 and Au_9 clusters containing NO_3^-) whereas the size of the cluster has a more pronounced effect (83.9 ± 0.1 eV for Au_{11} cluster containing Cl^-).[48]

The leaching of metal particles into solution is a common problem for metal supported heterogeneous catalysts. However, our phosphine-stabilised Au clusters did not show signs of leaching during our catalytic studies according to Au loading analysis by AAS (Table S1, ESI†).

3.2 Catalytic testing

The liquid phase oxidation of benzyl alcohol using gold nanoparticle-based catalysts reported here yielded benzoic acid and methyl benzoate as the major products, which were identified using HPLC-MS and quantified using HPLC-UV (using an internal standard and reference compound solutions of known concentration for calibration). The untreated catalysts with 0.17 wt% gold loading were inactive, showing no conversion while heat treated catalysts showed almost complete (>92%) conversion of benzyl alcohol after 4 hours (see Table 2). The most active catalysts gave very high catalytic activity with a molar substrate to metal ratio of 5800 and turnover frequency up to 0.65 s^{-1} (which is orders of magnitude greater than in any of the related earlier reports, Table S2 ESI†). There were several factors contributing to the high activity of our catalysts. Firstly, the water soluble base (K_2CO_3) is known to be a promoter in liquid phase oxidation of alcohols.[62,63] Rossi proposed that alcohols cannot adsorb directly onto gold and a base was required to deprotonate the hydroxyl group forming a metal alkoxide prior to adsorption onto gold.[22] The indispensable role of the base was shown when no conversion of benzyl alcohol was achieved in its absence (Table 1, entries 4–6). There are studies of benzyl alcohol oxidation using supported-gold catalysts under base-free conditions, nevertheless, in those studies, high conversions (>90%) were rarely achieved.[15,16,64] In some cases, high conversions of benzyl alcohol under base-free conditions were also reported, for example, Su *et al.* reported that gold nanoparticles supported on the binary mesostructured Ga–Al mixed oxide were able to catalyse benzyl alcohol under base-free conditions at 80 °C with a high conversion (98%).[65] Abad *et al.* employed Au/CeO_2 in the oxidation of various alcohols and observed high conversions under mild conditions.[66] Those authors suggested that the base was not required to deprotonate alcohols because the support contained active sites that were able to form cerium alkoxide, assisting the oxidation of alcohols.

Secondly, the nature of the support and metal–support interaction dictated the performance of the catalysts. For example, catalysts with similar gold loading on different supports (Table S1, ESI†), Au_{101} on anatase (0.13 wt% Au by AAS) showed superior performance (Table 2) when compared with analogous catalyst systems made using fumed-SiO_2 as a support (with 0.18 wt% Au by AAS). Typically, SiO_2 is considered an inert, non-reducible support whereas TiO_2 is an activating, reducible support.[67] The higher catalytic activity of Au/TiO_2 catalysts over Au/SiO_2 was also observed in CO oxidation in many studies.[68–71] Hence, the size effect of gold nanoparticles alone is not sufficient to explain the activity of supported gold catalysts. Metal–support interactions (MSI) play crucial role in defining reactivity and selectivity of supported gold catalysts. Haruta *et al.* and Baiker *et al.* hypothesized that the oxygen activation occurs at the perimeter (*i.e.* interface) of the gold nanoparticles and metal oxide supports.[72–74] This hypothesis could explain the lower activity of Au_{101}/SiO_2 catalysts as compared to Au_{101}/anatase in benzyl alcohol oxidation observed in this study, since silica based

Table 2 Performance of gold catalysts in the liquid phase oxidation of benzyl alcohol

Entry	Catalyst	Size (nm)	Time (h)	Conversion (%)	Selectivity to methyl benzoate (%)	Selectivity to benzoic acid (%)	TOF (s^{-1})
1	Blank[a,b]	n/a	4	0	0	0	0
2	Anatase[a,b]	n/a	4	0	0	0	0
3	Anatase[a]	n/a	4	0	0	0	0
4	0.17% Au_{101}/TiO_2-untreated[b]	2.0 ± 0.4	4	0	0	0	0
5	0.17% Au_{101}/TiO_2–O_2[b]	3.5 ± 0.8	4	0	0	0	0
6	0.17% Au_{101}/TiO_2–O_2–H_2[b]	4.4 ± 1.2	4	0	0	0	0
7	0.17% Au_{101}/TiO_2-untreated	2.0 ± 0.4	4	0	0	0	0
8	0.17% Au_{101}/TiO_2–O_2	3.5 ± 0.8	4	96	79	21	0.51
9	0.17% Au_{101}/TiO_2–O_2–H_2	4.4 ± 1.2	4	97	75	23	0.51
10	0.17% Au_{101}/TiO_2-untreated[c]	3.6 ± 1.2	4	29	65	15	0.12
11	0.17% Au_{101}/TiO_2–O_2[c]	3.9 ± 1.0	4	96	73	20	0.51
12	0.17% Au_{101}/TiO_2–O_2–H_2[c]	4.6 ± 1.5	4	98	70	23	0.51
13	0.01% Au_{101}/TiO_2-untreated[d]	<2[e]	4	0	0	0	0
14	0.01% Au_{101}/TiO_2–O_2[d]	<2[e]	4	0	0	0	0
15	0.01% Au_{101}/TiO_2–O_2–H_2[d]	<2[e]	4	0	0	0	0
16	1.3% Au_{101}/TiO_2-untreated	2.7 ± 0.6	4	99	87	13	0.05
17	0.17% Au_{101}/TiO_2–O_2	3.5 ± 0.8	3	93	78	22	0.65
18	0.17% Au_{101}/TiO_2–O_2–H_2	4.4 ± 1.2	3	92	76	24	0.65
19	0.17% Au_9/TiO_2-untreated	<2[e]	4	0	0	0	0
20	0.17% Au_9/TiO_2–O_2	2.4 ± 0.5	4	0	0	0	0
21	0.17% Au_9/TiO_2–O_2–H_2	2.9 ± 0.9	4	20	23	18	0.08
22	0.17% Au_{101}/SiO_2-untreated	<2[e]	4	0	0	0	0
23	0.17% Au_{101}/SiO_2–O_2	3.6 ± 2.7	4	69	72	24	0.25
24	0.17% Au_{101}/SiO_2–O_2–H_2	4.4 ± 2.5	4	69	70	26	0.26
25	0.5% Au_{101}/SiO_2-untreated	3.6 ± 1.2	4	63	74	16	0.09
26	0.5% Au_{101}/SiO_2–O_2	4.7 ± 1.6	4	95	63	31	0.13
27	0.5% Au_{101}/SiO_2–O_2–H_2	5.7 ± 2.9	4	99	65	32	0.14
28	0.17% Au_{101}/TiO_2–O_2 + KNO_3[f]	3.5 ± 0.8	4	85	78	21	0.46
29	0.17% Au_9/TiO_2–O_2 + KCl[f]	2.4 ± 0.5	4	0	0	0	0

Reaction conditions: 50 mg catalyst, 2.5 mmol benzyl alcohol, 25 mL methanol (solvent), 1.25 mmol anisole (internal standard), 2.5 mmol K_2CO_3, 5 bar O_2 pressure, 80 °C. [a] Without gold catalyst. [b] Without base (K_2CO_3). [c] Recycled catalysts. [d] 850 mg of a catalyst was used to retain the same total amount of gold as in the case of 0.17 wt% Au catalyst. [e] The size of gold nanoparticle was estimated from the absence of LSPR band in UV-vis DR spectrum. [f] KNO_3 (or KCl) was added according to equivalent molar percentage by impregnation method.

catalysts with much larger particles will have much smaller surface area corresponding to the gold–support interface. The high activity of heat treated catalysts can be attributed to stronger metal–support interaction established during calcination. Haruta *et al.* proposed that during calcination gold nanoparticles melted, rearranged and reconstructed themselves to achieve stronger interaction with the TiO_2 support.[75] This hypothesis is in line with the report by Buffat and Borel that 2 nm gold nanoparticles melt around 600 K,[76] which is significantly lower than the melting point of the bulk gold (1337 K). Wu *et al.* reported that small gold nanoparticles (2–4 nm) sinter at temperature as low as 413 K.[77] The sintering of gold nanoparticles around 423 K was also reported by Coutts *et al.*[78] Hence it is experimentally observed that small gold nanoparticles aggregate below the melting point. Analysis of supported-gold particle sizes as measured by TEM (Table 1) showed that the particle size distribution of gold nanoparticles was wider (indicated by larger standard deviation) on SiO_2 support as compared to TiO_2 for the same Au loading (target 0.17 wt%), suggesting that weaker metal–support interaction in Au_{101}/SiO_2 catalysts facilitates aggregation resulting in wider particle size distributions despite the significantly higher surface area of SiO_2 support.

For the same Au loading (0.17 wt%) and support (TiO_2), Au_{101} cluster-based catalysts showed much higher catalytic activity compared to Au_9-based catalysts even though the gold particles size were smaller in the case of Au_9/TiO_2 (*cf.* Au_{101}/TiO_2 analogues, Table 2, entries 19–21 *cf.* entries 4–6). We hypothesize that the presence of anionic species within the gold cluster (Cl^- in Au_{101} *vs.* NO_3^- in Au_9) strongly affect the catalytic activity. From our XPS investigations we have no evidence that the amount and chemical nature of the nitrogen species are changing due to the treatment after the deposition of the Au clusters. To identify the role of the component of the cluster precursor responsible for quenching of the catalytic activity, we investigated the role of such an anionic component in benzyl alcohol oxidation. Firstly, we added KCl, with the amount according to the weight percentage of Cl^- in $Au_{101}(PPh_3)_{21}Cl_5$ (0.08 wt%) to mimic the presence of Cl^- anion, to the catalyst and calcined it under O_2 to resemble Au_{101}/TiO_2–O_2; we found no increase in the catalytic activity (Table 2, entry 29 *cf.* entry 20). When KNO_3 (amount estimated to mimic the amount of NO_3^- from Au_9, 4.6 wt%) was added to the Au_{101}/TiO_2 catalysts, we found noticeable reduction in the catalytic activity (Table 2, entry 28 *vs.* 8). The nitrate is an integral part of the Au_9 cluster precursor used in

catalyst fabrication and would be perfectly positioned to affect gold particles, causing deactivation of the catalyst (Table 2, entries 19–21). For the Au_{101} based catalyst (Table 2, entry 28), the nitrate was introduced after the catalyst had been formed, which could limit the efficiency of the interaction of the nitrate with the gold particles and result in the moderate drop in activity. Hence, it appears that the presence of NO_3 lowers the catalytic activity of Au_{101}-based catalysts and could be the reason for the significantly lower activity of Au_9-based analogues. To the best of our knowledge this is the first report of the effect of NO_3^- on activity of gold-based heterogeneous catalysts. While numerous studies report that ultra-small gold nanoparticles (<2 nm) are the key active site,[23,26,79] our results demonstrate that the size of gold nanoparticles alone is not sufficient to explain the catalytic activity of catalysts made using phosphine-capped Au nanoparticles as it is considerably affected by the type of anions present in the supported gold cluster catalysts, type of support and activation treatment protocols. Quintanilla *et al.* investigated the effect of N-based compounds (dodecylamine *vs.* polyvinylpyrrolidone) as stabilizing agents for gold nanoparticles deposited onto γ-Al_2O_3 in benzyl alcohol oxidation.[80] The authors found that the polyvinylpyrrolidone-capped gold nanoparticles had higher catalytic activity than the dodecylamine-capped gold nanoparticles due to the reduced steric hindrance of the gold surface by the polymer, allowing access of the substrate to the surface of gold nanoparticles. However, in our case, the N-based compound is present as a counter anion (NO_3^-), not as a stabilizing agent. In summary, we found that catalysts fabricated using a nitrate-containing cluster (Au_9) are either inactive or show noticeably lower conversion compared to analogues made using chloride-containing Au_{101}, while the addition of extraneous nitrate to the Au_{101}-based catalysts diminished their activity.

The effect of different calcination conditions is negligible for Au_{101}-based catalysts but has significant impact on Au_9/TiO_2 catalysts (see Table 2). Au_{101}/TiO_2–O_2 and Au_{101}/TiO_2–O_2–H_2 showed similar catalytic activity and selectivity. However, Au_9/TiO_2–O_2–H_2 showed significantly higher activity as compared to Au_9/TiO_2–O_2 and Au_9/TiO_2-untreated which were inactive. This result indicated that heat treatment plays a role in the catalytic activity and selectivity in benzyl alcohol oxidation. Yuan *et al.* prepared Au_9/TiO_2 for CO oxidation.[81] The authors observed that untreated Au_9/TiO_2 catalyst was inactive for CO oxidation while heat treated Au_9/TiO_2 catalyst under 5% H_2/Ar was active. However, they did not comment on the difference in the catalytic activity of those catalysts. In the case of Au nanoparticles containing residual Cl^- species, calcination under H_2 atmosphere could remove Cl^- in the form of HCl, as proposed by Haruta *et al.*[82] However, at this stage we could not conclude the fate of NO_3^- species after combined O_2–H_2 calcination because the available XPS data provide no evidence about how the and nature of the nitrogen species changes after such calcination.

The proposed reaction pathway of benzyl alcohol oxidation in methanol in the presence of base is shown in Fig. 6.

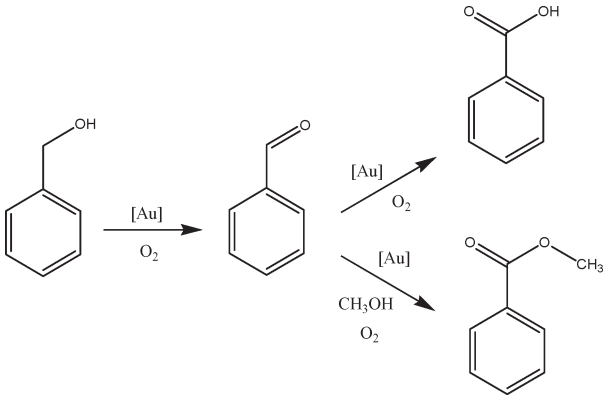

Fig. 6 Proposed reaction pathway of oxidation of benzyl alcohol in methanol.

Benzyl alcohol is first oxidized to benzaldehyde, which serves as an intermediate in this catalytic system. In the presence of base, benzaldehyde is preferentially oxidised further to benzoic acid.[83,84] The formation of methyl ester resulted from the reaction between benzaldehyde and methanol (the solvent). We carried out a control reaction using benzaldehyde and benzoic acid as substrates (instead of benzyl alcohol). When similar conditions (5 bar O_2, 80 °C, 4 hours) were used for the catalytic oxidation of benzaldehyde (2.5 mmol) in methanol (25 mL) using Au_{101}/anatase catalysts, a complete transformation of benzaldehyde to benzoic acid and methyl benzoate with the same distribution of products (*i.e.* benzoic acid : methyl benzoate of 70 : 30) was observed. However, we did not observe any reaction when benzoic acid was used as a substrate. Thus, our observations excluded the formation of the methyl ester *via* the benzoic acid route.

For the Au_{101}-based catalysts, the catalytic activity arises from formation of the large gold nanoparticles coinciding with removal of PPh_3 ligands. All untreated Au_{101}/TiO_2 (0.01 and 0.17 wt%) and Au_{101}/SiO_2 (0.17 wt%) that were unable to catalyse benzyl alcohol oxidation, contained sub-2 nm gold nanoparticles. In trying to explain this observation one has to consider effects of metal core properties and the possibility that a significant proportion of an otherwise reactive gold surface could be blocked by protective phosphine ligands. Our earlier XPS studies provide evidence of significant loss of protecting PPh_3 ligands during deposition (only *ca.* 10% of P XPS signal intensity remained, due to residual PPh_3 ligands) in the case of 0.17 wt% Au_{101}/TiO_2.[47] Although it is impossible to outright dismiss the argument that the residual 10% of ligands could completely deactivate the catalysts, one should attempt to find an alternative explanation. An earlier report by Valden *et al.* demonstrated an important transition from non-metallic to metallic properties occurring for *ca.* Au_{300} clusters on TiO_2.[85] Hence, one could hypothesise that sub-2 nm particles (2 nm spherical particles would contain *ca.* 250 atoms)[86] could be inactive, as observed in our reactions, due to their non-metallic state. The presence of non-metallic particles in these catalysts is further confirmed by our UV-vis DRS results (Table 1, entries 1 and 14). However,

untreated 1.3 wt% Au_{101}/TiO_2 (mean gold particle size of 2.7 ± 1.6 nm) and untreated 0.5% Au_{101}/SiO_2 (mean gold particle size of 3.6 ± 1.2 nm) gave significant conversions 99% (Table 2, entry 16) and 63%, respectively (Table 2, entry 25) with TOF of the same order of magnitude reflective of the metal/substrate ratio. This observation implies that in the case of highly metal-loaded Au_{101}-derived catalysts, the formation of larger, metallic nanoparticles (which is likely to coincide with even more pronounced loss of phosphine ligands during aggregation) could be responsible for the observed activity. The gold nanoparticles in Au_{101}/TiO_2 catalysts agglomerated slightly after the catalytic tests (Table 2). The ^{31}P NMR spectrum of the reaction mixture showed the presence of triphenylphosphine oxide, which was formed from the phosphine ligands dislodged from the gold core, which then oxidised during the catalytic reaction and dissolved in the catalytic reaction mixture. The Au_{101}/TiO_2-untreated catalyst was active upon recycling (*i.e.* in the 2nd consecutive catalytic test) and showed noticeably increased conversion (29%, Table 2, entry 10) compared to inactive fresh catalyst, and formed considerable amounts of benzaldehyde as compared to other catalytic tests in this study (Fig. S11†). Again, the increase in activity of the 0.17 wt% Au_{101}/TiO_2-untreated samples upon recycling could be attributed to an increase in size of the gold nanoparticles and the simultaneous loss of phosphine ligands from the gold core during the first catalytic test. However, comparison between the two catalysts with very similar *ca.* 3.5 nm particle sizes – 0.17 wt% Au_{101}/TiO_2 recycled (Table 2, entry 10) and activated by calcination under O_2 (Table 2, entry 5) shows that particle size is clearly not the only factor. It should be emphasized that the TEM imaging does not allow easy quantification of the density/number of Au particles per particle of support and such TEM-based sizing alone could miss the presence of an inactive population of TEM-invisible smaller particles. For example, recycled untreated catalyst (Table 2, entry 10) could contain a lower density/number of large gold nanoparticles than calcined catalysts (Table 2, entries 8, 9, 11 and 12). Yet, a possibly more important factor in explaining the observed differences could be the effect of the higher-temperature treatment under O_2 atmosphere which could form a better contact between the gold particles and the support, while PPh_3 removal from the gold core is even more pronounced when compared to the recycled catalysts. For example, Haruta *et al.* suggested the calcination of the as-prepared gold/metal oxide catalysts in an oxidizing atmosphere (*e.g.* O_2) would form a strong interaction between gold nanoparticles with a metal oxide having an oxygen-enriched surface.[87] Both heat treated Au_{101}/TiO_2 catalysts under O_2 and O_2–H_2 showed no significant loss of catalytic activity and selectivity after the first catalytic test.

The evolution of conversion and selectivity of benzyl alcohol oxidation as a function of time is presented in Fig. 7. The high conversion of benzyl alcohol (80–90%) was observed after the first two to three hours. The selectivity towards the formation of methyl benzoate and benzoic acid are independent of

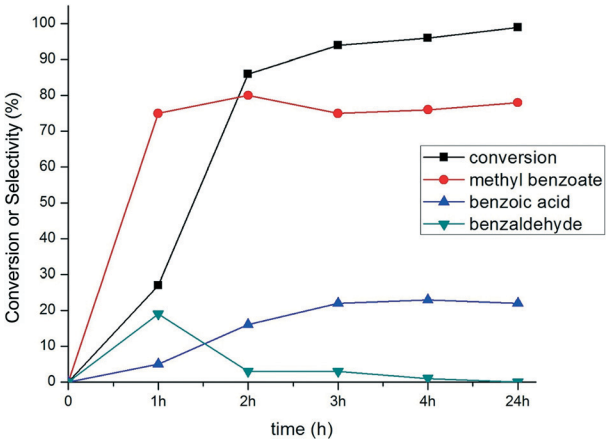

Fig. 7 Time-dependent profile of benzyl alcohol oxidation using 0.17% Au_{101}/TiO_2–O_2. Reaction conditions: 2.5 mmol benzyl alcohol, 25 mL methanol, 1.25 mmol anisole, 2.5 mmol K_2CO_3, 5 bar O_2, 80 °C.

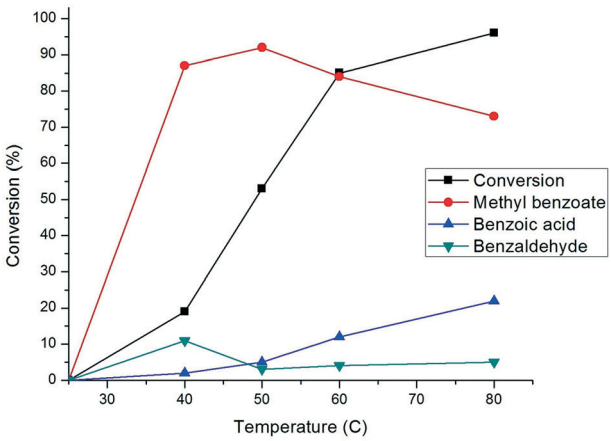

Fig. 8 The effect of temperature on the conversion and profile of benzyl alcohol oxidation products using 0.17% Au_{101}/TiO_2–O_2. Reaction conditions: 2.5 mmol benzyl alcohol, 25 mL methanol, 1.25 mmol anisole, 2.5 mmol K_2CO_3, 5 bar O_2, and 4 hours.

reaction time but primarily dependent on the reaction temperature, as shown in Fig. 8. A considerable amount (*ca.* 20%) of benzaldehyde was formed after one hour and then depleted over time (Fig. 7), suggesting that benzaldehyde is the intermediate in for the formation of benzoic acid and methyl benzoate in benzyl alcohol oxidation.[88–90] The effect of the temperature in this reaction was studied from room temperature (25 °C) up to 80 °C (Fig. 8). Reduction in the temperature of the catalytic reaction results in the reduction of the catalytic activity. However, the product selectivity shows non-linear behaviour. The highest selectivity towards methyl benzoate (93%) was observed at 50 °C with 53% conversion of benzyl alcohol, suggesting the selective formation of methyl benzoate is possible by manipulating the reaction temperature.

4 Conclusion

In summary, we report that high catalytic activity (conversions of >90%) is achieved using Au_{101}-based catalysts

whereas Au_9-based catalysts are barely active. In this study, we find that the catalytic performance in benzyl alcohol oxidation is determined by gold particle size, the type of the support and the counter anions present in the gold cluster composition. For Au_{101}-based catalysts on both TiO_2 and SiO_2, we observe that the catalytic activity appears with the formation of large (>2 nm) gold nanoparticles which coincides with the partial removal of phosphine ligands. We also observe the higher catalytic activity of TiO_2-supported catalysts as compared to that of SiO_2-supported catalysts, which could be due to the stronger metal–support interaction effect as proposed by Haruta. The effect of heat treatment under different atmospheres on catalytic performance is less pronounced in the case of Au_{101}/TiO_2 catalysts, but significantly affects Au_9/TiO_2 catalysts with noticeable catalytic activity (20% conversion) observed only for Au_9/TiO_2–O_2–H_2. The selectivity toward the formation of methyl benzoate can be tuned by manipulating the reaction temperature. The highest selectivity towards methyl benzoate was achieved at 50 °C with 93%.

Acknowledgements

The authors would like to thank Professor Milo Kral and Mike Flaws for their help with TEM, Alistair Duff for AAS measurements of the gold content in catalysts, Dr. Meike Holzenkaempfer and Dr. Marie Squire for development of the HPLC methodology, and Professor Bryce Williamson for valuable discussions and Dr. Sedigheh Ghadamgahi for help with initial optimization of catalytic test conditions. This work was supported by the MacDiarmid Institute, University of Canterbury and University of Malaya, Kuala Lumpur (UM High Impact Research Grant UM-MOHE UM.C/HIR/MOHE/SC/11) and Australian Synchrotron (AS112/SXR/4641) for XPS study on phosphine gold nanoparticles).

References

1 M. Haruta, T. Kobayashi, H. Sano and N. Yamada, *Chem. Lett.*, 1987, **16**, 405–408.
2 B. Nkosi, M. D. Adams, N. J. Coville and G. J. Hutchings, *J. Catal.*, 1991, **128**, 378–386.
3 M. Haruta and M. Daté, *Appl. Catal., A*, 2001, **222**, 427–437.
4 M. Haruta, *Angew. Chem., Int. Ed.*, 2014, **53**, 52–56.
5 M. Stratakis and H. Garcia, *Chem. Rev.*, 2012, **112**, 4469–4506.
6 T. Mallat and A. Baiker, *Annu. Rev. Chem. Biomol. Eng.*, 2012, **3**, 11–28.
7 N. Dimitratos, J. A. Lopez-Sanchez and G. J. Hutchings, *Chem. Sci.*, 2012, **3**, 20–44.
8 C. H. Christensen and J. K. Nørskov, *Science*, 2010, **327**, 278–279.
9 S. Mandal, K. K. Bando, C. Santra, S. Maity, O. O. James, D. Mehta and B. Chowdhury, *Appl. Catal., A*, 2013, **452**, 94–104.
10 C. Della Pina, E. Falletta and M. Rossi, *J. Catal.*, 2008, **260**, 384–386.
11 H. Miyamura, T. Yasukawa and S. Kobayashi, *Green Chem.*, 2010, **12**, 776–778.
12 V. Augugliaro and L. Palmisano, *ChemSusChem*, 2010, **3**, 1135–1138.
13 C. P. Vinod, K. Wilson and A. F. Lee, *J. Chem. Technol. Biotechnol.*, 2011, **86**, 161–171.
14 J. Kilmartin, R. Sarip, R. Grau-Crespo, D. Di Tommaso, G. Hogarth, C. Prestipino and G. Sankar, *ACS Catal.*, 2012, **2**, 957–963.
15 V. R. Choudhary, A. Dhar, P. Jana, R. Jha and B. S. Uphade, *Green Chem.*, 2005, **7**, 768–770.
16 V. R. Choudhary, R. Jha and P. Jana, *Green Chem.*, 2007, **9**, 267–272.
17 T. Mallat and A. Baiker, *Catal. Today*, 1994, **19**, 247–283.
18 P. Gallezot, *Catal. Today*, 1997, **37**, 405–418.
19 R. Garcia, M. Besson and P. Gallezot, *Appl. Catal., A*, 1995, **127**, 165–176.
20 J. H. J. Kluytmans, A. P. Markusse, B. F. M. Kuster, G. B. Marin and J. C. Schouten, *Catal. Today*, 2000, **57**, 143–155.
21 M. Besson and P. Gallezot, *Catal. Today*, 2000, **57**, 127–141.
22 L. Prati and M. Rossi, *J. Catal.*, 1998, **176**, 552–560.
23 Y. Liu, H. Tsunoyama, T. Akita and T. Tsukuda, *Chem. Lett.*, 2010, **39**, 159–161.
24 H. Tsunoyama, H. Sakurai, Y. Negishi and T. Tsukuda, *J. Am. Chem. Soc.*, 2005, **127**, 9374–9375.
25 P. Haider, B. Kimmerle, F. Krumeich, W. Kleist, J.-D. Grunwaldt and A. Baiker, *Catal. Lett.*, 2008, **125**, 169–176.
26 H. Tsunoyama, N. Ichikuni, H. Sakurai and T. Tsukuda, *J. Am. Chem. Soc.*, 2009, **131**, 7086–7093.
27 N. F. Zheng and G. D. Stucky, *J. Am. Chem. Soc.*, 2006, **128**, 14278–14280.
28 Y. Liu, H. Tsunoyama, T. Akita, S. Xie and T. Tsukuda, *ACS Catal.*, 2010, **1**, 2–6.
29 U. Hartfelder, C. Kartusch, M. Makosch, M. Rovezzi, J. Sa and J. A. van Bokhoven, *Catal. Sci. Technol.*, 2013, **3**, 454–461.
30 Q. Zhang, W. Deng and Y. Wang, *Chem. Commun.*, 2011, **47**, 9275–9292.
31 A. Villa, D. Wang, D. S. Su and L. Prati, *ChemCatChem*, 2009, **1**, 510–514.
32 R.-Y. Zhong, X.-H. Yan, Z.-K. Gao, R.-J. Zhang and B.-Q. Xu, *Catal. Sci. Technol.*, 2013, **3**, 3013–3019.
33 K. Y. Lee, Y. W. Lee, J.-H. Lee and S. W. Han, *Colloids Surf., A*, 2010, **372**, 146–150.
34 A. Kulkarni, R. J. Lobo-Lapidus and B. C. Gates, *Chem. Commun.*, 2010, **46**, 5997–6015.
35 X. Nie, C. Zeng, X. Ma, H. Qian, Q. Ge, H. Xu and R. Jin, *Nanoscale*, 2013, **5**, 5912–5918.
36 G. Li, C. Liu, Y. Lei and R. Jin, *Chem. Commun.*, 2012, **48**, 12005–12007.
37 G. Li, H. Qian and R. Jin, *Nanoscale*, 2012, **4**, 6714–6717.
38 Y. Zhu, H. Qian and R. Jin, *Chem. – Eur. J.*, 2010, **16**, 11455–11462.
39 Y. Zhu, H. Qian, B. A. Drake and R. Jin, *Angew. Chem., Int. Ed.*, 2010, **49**, 1295–1298.

40 P. Huang, G. Chen, Z. Jiang, R. Jin, Y. Zhu and Y. Sun, *Nanoscale*, 2013, **5**, 3668–3672.
41 G. Li, C. Zeng and R. Jin, *J. Am. Chem. Soc.*, 2014, **136**, 3673–3679.
42 Y. Liu, H. Tsunoyama, T. Akita and T. Tsukuda, *Chem. Commun.*, 2010, **46**, 550–552.
43 V. G. M. Turner, P. Abdulkin, B. F. G. Johnson and R. M. Lambert, *Nature*, 2008, **454**, 981–983.
44 B. G. Donoeva, D. S. Ovoshchnikov and V. B. Golovko, *ACS Catal.*, 2013, **3**, 2986–2991.
45 D. S. Ovoshchnikov, B. G. Donoeva, B. E. Williamson and V. B. Golovko, *Catal. Sci. Technol.*, 2014, **4**, 752–757.
46 G. H. Woehrle, L. O. Brown and J. E. Hutchison, *J. Am. Chem. Soc.*, 2005, **127**, 2172–2183.
47 D. P. Anderson, R. H. Adnan, J. F. Alvino, O. Shipper, B. Donoeva, J.-Y. Ruzicka, H. Al Qahtani, H. H. Harris, B. Cowie, J. B. Aitken, V. B. Golovko, G. F. Metha and G. G. Andersson, *Phys. Chem. Chem. Phys.*, 2013, **15**, 14806–14813.
48 D. P. Anderson, J. F. Alvino, A. Gentleman, H. A. Qahtani, L. Thomsen, M. I. J. Polson, G. F. Metha, V. B. Golovko and G. G. Andersson, *Phys. Chem. Chem. Phys.*, 2013, **15**, 3917–3929.
49 V. Peneau, Q. He, G. Shaw, S. A. Kondrat, T. E. Davies, P. Miedziak, M. Forde, N. Dimitratos, C. J. Kiely and G. J. Hutchings, *Phys. Chem. Chem. Phys.*, 2013, **15**, 10636–10644.
50 A. Villa, D. Wang, G. M. Veith, F. Vindigni and L. Prati, *Catal. Sci. Technol.*, 2013, **3**, 3036–3041.
51 *Handbook of Preparative Inorganic Chemistry*, ed. G. Brauer, Academic Press, NY, 1963, vol. 1.
52 W. W. Weare, S. M. Reed, M. G. Warner and J. E. Hutchison, *J. Am. Chem. Soc.*, 2000, **122**, 12890–12891.
53 F. Wen, U. Englert, B. Gutrath and U. Simon, *Eur. J. Inorg. Chem.*, 2008, **2008**, 106–111.
54 A. A. Herzing, C. J. Kiely, A. F. Carley, P. Landon and G. J. Hutchings, *Science*, 2008, **321**, 1331–1335.
55 R. Balasubramanian, R. Guo, A. J. Mills and R. W. Murray, *J. Am. Chem. Soc.*, 2005, **127**, 8126–8132.
56 P. V. Kamat, *J. Phys. Chem. B*, 2002, **106**, 7729–7744.
57 S. Link and M. A. El-Sayed, *Annu. Rev. Phys. Chem.*, 2003, **54**, 331–366.
58 E. A. Coronado, E. R. Encina and F. D. Stefani, *Nanoscale*, 2011, **3**, 4042–4059.
59 R. Fenger, E. Fertitta, H. Kirmse, A. F. Thunemann and K. Rademann, *Phys. Chem. Chem. Phys.*, 2012, **14**, 9343–9349.
60 N. R. Jana, L. Gearheart and C. J. Murphy, *Langmuir*, 2001, **17**, 6782–6786.
61 C. Yang, Y. Zhou, G. An and X. Zhao, *Opt. Mater.*, 2013, **35**, 2551–2555.
62 J. Yang, Y. Guan, T. Verhoeven, R. van Santen, C. Li and E. J. M. Hensen, *Green Chem.*, 2009, **11**, 322–325.
63 N. Zheng and G. D. Stucky, *Chem. Commun.*, 2007, 3862–3864.
64 T. Ishida, M. Nagaoka, T. Akita and M. Haruta, *Chem. – Eur. J.*, 2008, **14**, 8456–8460.
65 F.-Z. Su, Y.-M. Liu, L.-C. Wang, Y. Cao, H.-Y. He and K.-N. Fan, *Angew. Chem., Int. Ed.*, 2008, **47**, 334–337.
66 A. Abad, P. Concepción, A. Corma and H. García, *Angew. Chem., Int. Ed.*, 2005, **44**, 4066–4069.
67 M. M. Schubert, S. Hackenberg, A. C. van Veen, M. Muhler, V. Plzak and R. J. Behm, *J. Catal.*, 2001, **197**, 113–122.
68 S. D. Lin, M. Bollinger and M. A. Vannice, *Catal. Lett.*, 1993, **17**, 245–262.
69 H. Zhu, Z. Ma, J. C. Clark, Z. Pan, S. H. Overbury and S. Dai, *Appl. Catal., A*, 2007, **326**, 89–99.
70 S. H. Overbury, L. Ortiz-Soto, H. Zhu, B. Lee, M. Amiridis and S. Dai, *Catal. Lett.*, 2004, **95**, 99–106.
71 L. Delannoy, N. El Hassan, A. Musi, N. N. Le To, J.-M. Krafft and C. Louis, *J. Phys. Chem. B*, 2006, **110**, 22471–22478.
72 M. Haruta, *Chem. Rec.*, 2003, **3**, 75–87.
73 M. Daté, M. Okumura, S. Tsubota and M. Haruta, *Angew. Chem., Int. Ed.*, 2004, **43**, 2129–2132.
74 J.-D. Grunwaldt and A. Baiker, *J. Phys. Chem. B*, 1999, **103**, 1002–1012.
75 S. Tsubota, T. Nakamura, K. Tanaka and M. Haruta, *Catal. Lett.*, 1998, **56**, 131–135.
76 P. Buffat and J. P. Borel, *Phys. Rev. A: At., Mol., Opt. Phys.*, 1976, **13**, 2287–2298.
77 Y. Wu, Y. Li, P. Liu, S. Gardner and B. S. Ong, *Chem. Mater.*, 2006, **18**, 4627–4632.
78 M. J. Coutts, M. B. Cortie, M. J. Ford and A. M. McDonagh, *J. Phys. Chem. C*, 2009, **113**, 1325–1328.
79 Y. Liu, H. Tsunoyama, T. Akita and T. Tsukuda, *J. Phys. Chem. C*, 2009, **113**, 13457–13461.
80 A. Quintanilla, V. C. L. Butselaar-Orthlieb, C. Kwakernaak, W. G. Sloof, M. T. Kreutzer and F. Kapteijn, *J. Catal.*, 2010, **271**, 104–114.
81 Y. Yuan, K. Asakura, H. Wan, K. Tsai and Y. Iwasawa, *Catal. Lett.*, 1996, **42**, 15–20.
82 M. Haruta, *CATTECH*, 2002, **6**, 102–115.
83 S. E. Davis, M. S. Ide and R. J. Davis, *Green Chem.*, 2013, **15**, 17–45.
84 C. Bianchi, F. Porta, L. Prati and M. Rossi, *Top. Catal.*, 2000, **13**, 231–236.
85 M. Valden, X. Lai and D. W. Goodman, *Science*, 1998, **281**, 1647–1650.
86 C. L. Cleveland, *Phys. Rev. Lett.*, 1997, **79**, 1873–1876.
87 M. Haruta, S. Tsubota, T. Kobayashi, H. Kageyama, M. J. Genet and B. Delmon, *J. Catal.*, 1993, **144**, 175–192.
88 C. Marsden, E. Taarning, D. Hansen, L. Johansen, S. K. Klitgaard, K. Egeblad and C. H. Christensen, *Green Chem.*, 2008, **10**, 168–170.
89 A. B. Powell and S. S. Stahl, *Org. Lett.*, 2013, **15**, 5072–5075.
90 W. Cui, M. Jia, W. Ao and B. Zhaorigetu, *React. Kinet., Mech. Catal.*, 2013, **110**, 437–448.